Characterization of the coherent scattering induced by ridging patterns in agriculture by the use of polarimetric SAR imagery

Article *in* International Journal of Remote Sensing · June 2017

DOI: 10.1080/01431161.2017.1297545

CITATIONS
5

READS
184

6 authors, including:

Lingli Zhao
Wuhan University
33 PUBLICATIONS **212** CITATIONS
SEE PROFILE

Xin Huang
Wuhan University
163 PUBLICATIONS **4,500** CITATIONS
SEE PROFILE

Lei Shi
Wuhan University
35 PUBLICATIONS **256** CITATIONS
SEE PROFILE

Liangpei Zhang
Wuhan University
699 PUBLICATIONS **16,493** CITATIONS
SEE PROFILE

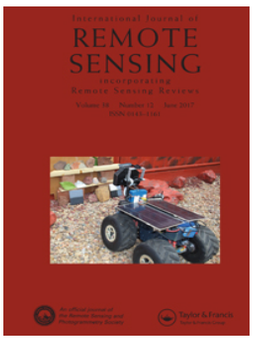

International Journal of Remote Sensing

ISSN: 0143-1161 (Print) 1366-5901 (Online) Journal homepage: http://www.tandfonline.com/loi/tres20

Characterization of the coherent scattering induced by ridging patterns in agriculture by the use of polarimetric SAR imagery

Lingli Zhao, Jie Yang, Pingxiang Li, Xin Huang, Lei Shi & Liangpei Zhang

To cite this article: Lingli Zhao, Jie Yang, Pingxiang Li, Xin Huang, Lei Shi & Liangpei Zhang (2017) Characterization of the coherent scattering induced by ridging patterns in agriculture by the use of polarimetric SAR imagery, International Journal of Remote Sensing, 38:12, 3502-3518, DOI: 10.1080/01431161.2017.1297545

To link to this article: http://dx.doi.org/10.1080/01431161.2017.1297545

INTERNATIONAL JOURNAL OF REMOTE SENSING, 2017
VOL. 38, NO. 12, 3502–3518
http://dx.doi.org/10.1080/01431161.2017.1297545

Taylor & Francis
Taylor & Francis Group

Characterization of the coherent scattering induced by ridging patterns in agriculture by the use of polarimetric SAR imagery

Lingli Zhao[a], Jie Yang[b], Pingxiang Li[b], Xin Huang[a], Lei Shi[c] and Liangpei Zhang[b]

[a]School of Remote Sensing and Information Engineering, Wuhan University, Wuhan, China; [b]The State Key Laboratory of Information Engineering in Surveying, Mapping, and Remote Sensing, Wuhan University, Wuhan, China; [c]Department of Land Surveying and Geo-Informatics, The Hong Kong Polytechnic University, Hung Hom, Hong Kong

ABSTRACT

This article investigates the scattering characteristics of ridging patterns in agriculture by the use of C-band polarimetric synthetic aperture radar (PolSAR) images. The polarimetric signatures of periodic potato fields and row wheat in different directions are highlighted using a set of polarimetric parameters. Enhanced coherent scattering is observed when the alignment direction of the ridging patterns is perpendicular to the radar's line of sight (LOS). The dominant backscattering mechanism of the ridging patterns is deduced by evaluating different polarimetric parameters. The increased copolarized backscattering coefficients and copolarized correlation coefficient, and the reduced entropy and polarimetric alpha angle, indicate a strong contribution of odd scattering to ridging patterns aligned perpendicular to the LOS. We also compare the dominant contributions to the backscattering of ridging patterns in different phenological stages. Although the canopy changes of potato and wheat with time are significant, the underlying periodic surface changes the dominant scattering mechanism of potato fields over all the phenological stages, and the wheat aligned parallel with the flight direction of radar still has relatively high coherent scattering in the different vegetation development stages. The variability analyses undertake in this study allow a more detailed documentation of the physical scattering process of the ridging patterns in agriculture, and will improve the applicability of synthetic aperture radar images in agriculture.

ARTICLE HISTORY
Received 24 May 2016
Accepted 15 February 2017

1. Introduction

Synthetic aperture radar (SAR) can be used to monitor the Earth in a reliable, continuous, and global way due to its capability of operating independently of daylight and weather conditions. Polarimetric SAR (PolSAR) has been the subject of increasing interest in crop monitoring due to the sensitivity of the rich multi-channel information to crop structure

CONTACT Lingli Zhao zhaolingli@whu.edu.cn School of Remote Sensing and Information Engineering, Wuhan University, Wuhan, China

and physical parameters (Lee and Pottier 2009; Moreira et al. 2013). In recent years, many supervised and unsupervised classification algorithms have been developed for PolSAR data, which allow the fine discrimination of different crops (Lee, Grunes, and De Grandi 1999; Xie et al. 2015; Zeyada et al. 2016). Furthermore, the inversion of physical and geophysical parameters has also been improved by refined description of the scattering of vegetation canopy using polarimetric combination or decomposition (Hajnsek et al. 2009; Jagdhuber et al. 2013; Ponnurangam et al. 2016). Meanwhile, phenological stages estimation of crops by the use of PolSAR (Corcione et al. 2016; Lopez–Sanchez, Cloude, and Ballester–Berman 2012; Mascolo et al. 2015, 2016) has promoted the application of SAR in precision farming.

In these studies, homogeneous incoherent scattering is often assumed for distributed targets to simplify the interpretation of backscattering (vanZyl and Kim 2011; Hosseini et al. 2015). However, the variability caused by the fields' management methods or imaging parameters hinders the assessments of crop growth, the separability of crops and the inversion of physical parameters. One common factor for such variability lies in the coherent scattering caused by ridging patterns, such as those found in periodic fields and row crops. It has been reported that ridging patterns have unfavourable effects on soil moisture inversion and crop growth monitoring (He et al. 2016; Wegmüller et al. 2006).

The sensitivity of ridging patterns' backscattering to the look direction of radar has been discussed in several studies (Brunfeldt and Ulaby 1986; Ouchi, Niiuchi, and Mohri 1999; Rosenqvist 1999; Zhao et al. 2014a). When the line of sight (LOS) is perpendicular to the alignment direction of the ridging patterns, enhanced copolarized backscattering coefficients have been observed in rice (Ouchi, Niiuchi, and Mohri 1999; Rosenqvist 1999), corn (Brunfeldt and Ulaby 1986), and harvested crop swath (Zhao et al. 2014a). Wegmüller et al. (2006, 2011) also observed the directional scattering of the 'flashing fields' effect over periodic fields, and Bragg resonance was believed to have occurred for the periodic surface. The variation of backscattering with the azimuthal look angle has been identified by sub-aperture decomposition (Ferro–Famil et al. 2003; Wegmüller et al. 2011). The problematic subapertures for data acquired with a large azimuth beamwidth have also been identified to minimize the influence of the variation in conventional PolSAR data analysis.

Some models have also been developed to simulate the scattering of the ridging patterns. Auquiere et al. (1997) developed the directional water cloud model to simulate the scattering changes of maize in different row directions. Theoretical models of periodic fields, such as the periodic integral equation model (PIEM, Ulaby et al. 2014) and the Shin–Kong models (Shin and Kong 1984; Mattia 2011), have also been used to describe the directional scattering. The periodic field can be considered to be the overlay between the rough surface and the periodic structure. The scattering of the periodic field is modelled as the convolution of the incoherent scattering from the quasi-random surface and the coherent scattering from the periodic structure. Although the models can describe the enhanced coherent scattering to some extent, the simulation accuracy of backscattering often varies a great deal, due to the limited understanding of the interaction between the signal and ridging patterns. In addition, the concomitant coherent and incoherent scattering in agricultural monitoring make the interpretation of the scattering mechanism difficult.

Motivated by the scattering characterization and the effect of directional coherent scattering on the monitoring of agriculture, we documented the scattering characteristics of ridging patterns by the use of a set of polarimetric signatures. Two examples of periodic potato fields and winter wheat in different directions were used to investigate the common features of coherent scattering. Furthermore, a series of polarimetric SAR images were used to investigate the effect of coherent scattering on crop growth monitoring.

2. Method

2.1. *Study area*

The study area of periodic potato fields is located in the Yigen farmland of Erguna City in Inner Mongolia, centred at 50° 22′ N and 120° 48′ E. The potato fields in Yigen farmland are all ridged, and the ridge heights change with the potato management activities. The study area of winter wheat is located in one of the agricultural demonstration areas of Dingxing County, Hebei Province, centred at 39° 11′ N and 115° 43′ E. The wheat in this area is all planted in rows by sowing machines.

2.2. *Satellite dataset acquisitions and preprocessing*

Eleven Radarsat-2 images in fine quad mode were acquired over the two study areas. Five fully polarimetric SAR images in FQ 18 with an incidence angle of 37° were acquired for the potato fields from 23 May 2013 to 27 August 2013, with an acquisition every 24 days in Yigen. Two images with a small incidence angle of 21° were first acquired during the jointing and milking stages of winter wheat in 2009, and another four polarimetric images with large incidence angles were acquired during the growth cycle of winter wheat in 2013. The configuration parameters (Morena, James, and Beck 2004) of these acquisitions are shown in Table 1. Figures 1 and 2) are the pseudo-colour red–green–blue (RGB) images composited by the different temporal SAR data for Yigen and Dingxing, respectively.

Two free tools, the PolSARpro SAR Data Processing and Educational Tool (http://earth.eo.esa.int/polsarpro/) and the Next ESA SAR Toolbox (NEST, http://nest.array.ca/web/nest), were used for the preprocessing of the SAR datasets. These tools are both open-source software packages developed under the direction of ESA. A 7×7 Lee filter (Lee, Grunes, and De Grandi 1999) was first used to suppress the speckle noise of the SAR images. Geometric correction was achieved using a range-Doppler model, with the assistance of an SRTM DEM with a 90 m resolution (http://srtm.csi.cgiar.org/). The registration of the geometrically corrected images was undertaken using the NEST tool for both the Dingxing and Yigen datasets. The results yielded root-mean-square errors (RMSEs) of less than one pixel in both the x and y directions for the registered images.

2.3. *Ground measurements*

Detailed *in situ* measurements were collected approximately synchronous with the Radarsat-2 image acquisitions. Snapshots of the potato and wheat crops in these

Table 1. Configuration parameters of the acquisitions, the phenological stages of the crops, and the related rainfall of 5 days before the acquisition of each image.

Acquisition time (DoY)	Incidence angle (°)	Orbit	Local time	Rainfall 5 days (mm)	Phenological stages of potato and winter wheat
Yigen, Inner Mongolia					
23 May 2013 (174)	37	A	6:22 pm	6.9	Unseeded
16 June 2013 (198)	37	A	6:22 pm	34.5	Sprouting
10 July 2013 (222)	37	A	6:22 pm	56.4	Leaf development and inflorescence emergence
3 August 2013 (246)	37	A	6:22 pm	25.0	Fruit development and filling
27 August 2013 (270)	37	A	6:22 pm	4.9	Ripening and senescence
Dingxing, Hebei					
26 April 2009 (80)	21	A	6:27 am	5.1	Booting and heading
26 May 2009 (104)	21	D	6:09 pm	11.3	Flowering and ripening
21 March 2013 (116)	44	A	6:22 pm	0.2	Germination and start of tillering
14 April 2013 (135)	44	A	6:22 pm	0.0	Tillering and start of jointing
15 May 2013 (146)	41	A	6:17 pm	0.0	Flowering
1 June 2013 (152)	44	A	6:22 pm	4.4	Filling and milking

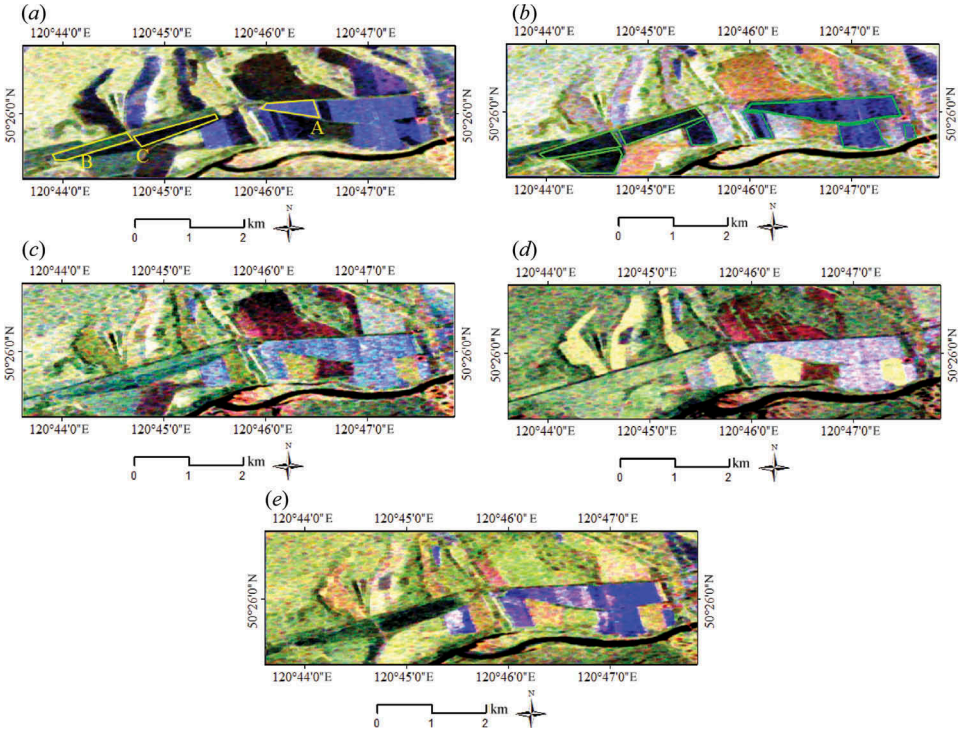

Figure 1. Pauli-RGB images are composited by $|S_{HH} - S_{VV}|^2$ (red), $|S_{HH} + S_{VV}|^2$ (blue), and $|S_{HV}|^2$ (green) for (a) 23 May 2013, (b) 16 June 2013, (c) 10 July 2013, (d) 3 August 2013, and (e) 27 August 2013. The polygons in (a) are the sizes of the three ROIs A, B, and C. The polygons in (b) are the *in situ* measured periodic potato fields in different directions. The polygons in dark and bright green are fields in perpendicular and parallel directions, respectively.

acquisitions are presented in Figure 3(a,b). The ridging directions of the potato fields and wheat fields were measured by GPS. The orientation angles of the ridges were computed using the row direction and the look direction of the Radarsat-2 images. The two orientations of $\theta = 0^\circ$ and $\theta = 90^\circ$ are referred to as the LOS being parallel with and

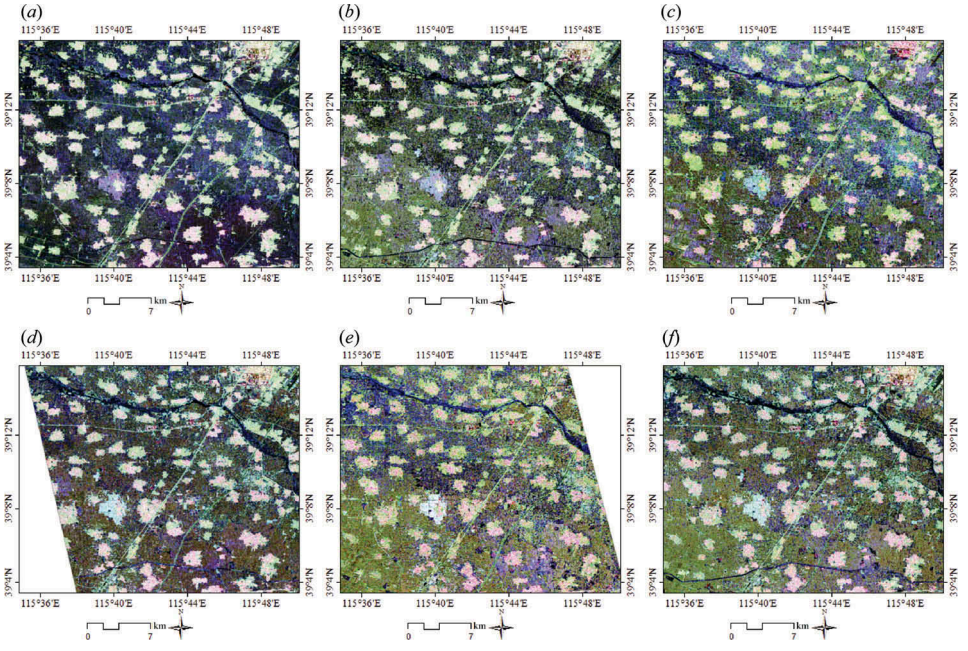

Figure 2. Pauli-RGB images are composited by $|S_{HH} - S_{VV}|^2$ (red), $|S_{HH} + S_{VV}|^2$ (blue), and $|S_{HV}|^2$ (green) for (a) 21 March 2013, (b) 14 April 2013, (c) 26 April 2009, (d) 15 May 2013, (e) 26 May 2009 and (f) 1 June 2013.

Figure 3. Snapshots of (a) the potato fields and (b) the wheat in Radarsat-2 image acquisitions over the two study areas.

perpendicular to the row direction of the ridging patterns, respectively. The row directions of regions of interests (ROIs) A and B over the potato fields in Figure 1(a) are parallel with and perpendicular to the LOS, respectively. ROI C was unploughed and flat on 23 May 2013. All the fields had similar soil moisture contents because they are all rain-fed fields. Table 2 lists the *in situ* measurements of the two bare periodic potato

Table 2. *In situ* measurements of the two bare periodic potato fields on 23 May 2013.

	Root-mean-square height (cm)	Correlation length (cm)	Height of periodic surface (cm)	Width of periodic surface (cm)	GSM (g cm^{-3})
A	1.42	2.71	20.0	68.2	17.34
B	1.15	3.06	22.0	67.8	21.11

fields on 23 May 2013. The ridging patterns of the periodic fields had similar surface parameters because of the use of the same tillering method.

2.4. *Polarimetric signatures*

A set of polarimetric signatures are presented to delineate the scattering of the ridging patterns in each growth stage. The expressions of the polarimetric parameters are listed in Table 3. Backscattering coefficients (σ^0_{HH}, σ^0_{HV} and σ^0_{VV}) are the basic information carried by SAR images. Span is the total backscattering. The copolarized ratio (γ) is also an indicator for vegetation growth (Manninen et al. 2013), but it is affected by the differential extinctions caused by canopy structure (Cloude 2009). The copolarized correlation coefficient (r_{HHVV}) between HH and VV measures the spatial elements' scattering randomness or the attenuation of the scattering medium (Lopez–Sanchez, Cloude, and Ballester–Berman 2012). A low copolarized phase difference (CPD) suggests a medium dominated by surface or volume scattering (Lee and Pottier 2009; Mcnairn et al. 2002). Three parameters – entropy (H), alpha (α), and anisotropy (A) – are derived from eigenvalue decomposition of the coherency matrix (Cloude and Pottier 1997). H, ranging from 0 and 1, describes the scattering randomness; α lies between 0° and 90°, indicating the dominant scattering mechanism; and A, ranging from 0 and 1, represents the relative power of the second and third scattering mechanisms.

2.5. *Importance assessment of the polarimetric signatures by the use of Random Forests (RFs)*

We classified the ridging patterns into parallel or perpendicular directions by the use of an RF classifier (Breiman 2001) and multi-temporal images. The sensitivity of the polarimetric signatures to the ridging patterns was assessed by the importance scores derived

Table 3. Expressions and physical descriptions of the polarimetric parameters.

Polarimetric parameters	Expressions	Physical descriptions
σ^0_{HH}, σ^0_{HV}, σ^0_{VV}	$\sigma^0_X = 10\log_{10}(\lvert S_X\rvert^2)$	Backscattering coefficients of the HH, HV, and VV polarizations
span	$\text{span} = 10\log_{10}(\lvert S_{HH}\rvert^2 + \lvert S_{VV}\rvert^2 + 2\lvert S_{HV}\rvert^2)$	Total backscattering
γ	$\gamma = \sigma^0_{HH} - \sigma^0_{VV}$	Copolarized ratio of HH and VV
$r = \lvert r_{HHVV}\rvert$	$\lvert r_{HHVV}\rvert = \left\lvert \langle S_{HH}S^*_{VV}\rangle / \sqrt{\langle\lvert S_{HH}\rvert^2\rangle\langle\lvert S_{VV}\rvert^2\rangle}\right\rvert$	Copolarized correlation coefficient between HH and VV
CPD	$\text{CPD} = \arg(\langle S_{HH}S^*_{VV}\rangle)$	Copolarized phase difference
H, a, A	$H = \sum -p_i \log_3 p_i,\ p_i = \lambda_i / \sum \lambda_k$ $A = (\lambda_2 - \lambda_3)/(\lambda_2 + \lambda_3)$, with $\lambda_1\ \lambda_2\ \lambda_3$	Entropy, alpha, and anisotropy derived from Cloude decomposition. λ_i are eigenvalues of the coherency matrix

from the RF classifier. We made use of a two-step hierarchical classification method to identify the winter wheat in different directions, because the wheat fields did not have clear boundaries with other land covers. First, the image was classified into multiple classes using the RF classifier. The area classified as wheat was then further classified into parallel or perpendicular directions using the series of images acquired in 2013. The crop fields showed clear boundaries in the Yigen farmland. The periodic potato fields were directly classified into two classes of potato in parallel direction and potato in perpendicular direction, using the series of images acquired in 2013.

The RF algorithm (Breiman 2001) is an ensemble classifier that has been successfully applied in land-cover mapping using multi-temporal or multi-source remote-sensing data (Barrett et al. 2014; Zhao et al. 2014b). The classifier builds many decision trees based on bootstrapped samples of the training data. 'Bagging' and random selection of the features are combined to control the variation of the training. Two user-defined parameters are the number of trees (k) and the number of variables (m) used to spilt the nodes. The number of trees should be taken large enough in order to allow for the convergence of the out-of-bag error (oob error) (Breiman 2001; Loosvelt et al. 2012). Here $k = 1000$, and $m = 5$. The parameter m can be optimized by means of minimizing the oob error. The classifier can be trained on high-dimensional data, without significant overfitting. In addition, it does not depend on the distribution of the data, and can tolerate a significant amount of noise. These properties are favourable for the classification of SAR data.

Normalization of features is not necessary for RFs. In addition, the importance of the variables can be assessed using the importance measures from RF (Loosvelt et al. 2012; Zhao et al. 2014b). We used the permutation importance to assess the contribution of the polarimetric signatures to wheat row direction. The permutation importance describes the difference in predication accuracy before and after permuting the variable of interest, averaged over all trees. It takes into account the impact of each predictor variable individually as well as its interaction with the other input variables. It can show the discrimination capability of the input features to separate the classes (Loosvelt et al. 2012; Zhao et al. 2014b). To reduce the bias, the classifications of potato and wheat by RF were conducted by randomly selecting 20% of the ground truth as the training samples. The remaining 80% were regarded as the test samples.

3. Results and analysis

3.1. *The scattering characteristics of the ridging patterns*

The periodic potato fields and winter wheat in different directions are taken as two examples of ridging patterns. In this section, differences in the angular behaviours of the polarimetric signatures caused by the direction of the ridging patterns are investigated.

3.1.1. *The scattering characteristics of the ridging pattern induced by periodic potato fields*

Table 4 lists the means and variances of the backscattering coefficients of the selected ROIs A, B, and C on 23 May 2013. It can be seen that there are significantly different

Table 4. Means and variances of the backscattering coefficients of the potato fields in different patterns on 23 May 2013.

Field	HH (mean ± variance (dB))	VV (mean ± variance (dB))	HV (mean ± variance (dB))
A	−8.08 ± 1.57	−8.31 ± 1.24	−23.65 ± 0.97
B	−14.62 ± 0.98	−14.55 ± 0.75	−23.38 ± 0.97
C	−16.76 ± 0.89	−16.54 ± 0.89	−28.87 ± 1.06

backscattering coefficients between periodic fields A and B. The σ_{HH} and σ_{VV} of field A are about 8 dB higher than those of field B. The signals from the individual ridges result in strong coherent scattering when the row direction of the periodic surface is perpendicular to the LOS. The σ_{HH} and σ_{VV} of field C are about 2 dB lower than those of periodic field B, which indicates that the ridging pattern has a weak effect on the backscattering of the parallel-aligned fields. The two periodic fields all have similar values of σ_{HV}, which is associated with incoherent scattering. The unploughed field C has a lower σ_{HV} than the other two fields, because of its small surface roughness. The differences in their backscattering coefficients indicate that the row direction of the ridging pattern is the critical factor for coherent scattering, but it has little effect on incoherent scattering.

We also investigated the effect of coherent scattering on the growth monitoring of crops. When a periodic surface is covered with a crop canopy, the backscattering is more complex. The total backscattering consists of three main parts: the scattering from the field surface, the scattering from the canopy and the scattering from the interaction between the canopy and the land surface.

Figure 4(a) shows the backscattering coefficients of periodic potato fields in different directions at several phenological stages. We can see that the evolution profiles of the backscattering coefficients of perpendicular-aligned field show similar trends to those of the parallel-aligned field. The σ_{HH},σ_{VV} and σ_{HV} all increase with the development of the potato canopy. The difference between and, namely copolarized ratio, does not have significant increase with potato growth, because the potato canopy does not has clear horizon or vertical structure during the crop growth stages, and the differential extinction is small (Cloude 2009; Lopez–Sanchez, Cloude, and Ballester–Berman 2012). However, the backscattering coefficients of σ_{HH} and σ_{VV} of the perpendicular fields are always higher than those of the ridged fields in the parallel direction. The σ_{HV}, which has a close relationship with the biomass of the canopy and crop seasonal changes (Ferrazzoli et al. 1997; Moran et al. 2012), increases with the growth of the potato plants and is insusceptible to the ridging pattern.

The σ_{HH} and σ_{VV} between the perpendicular-aligned and the parallel-aligned fields have the largest difference at the stage of 23 May 2013 when the fields were bare and their periodic amplitudes were high. The amplitude of the periodic surface at 16 June 2013 (DoY 198) is reduced, due to the sowing of the potato plants and the effect of rain, as shown by the snapshots in Figure 3(a). The low entropy and larger than indicate the dominated scattering mechanism for these fields at 16 June 2013 is Bragg scattering (Lee and Pottier 2009). When the ridges were made high again, the coherent scattering increased in the later stages. This suggests that the potato canopy does not destroy the coherent scattering from the periodic surface. The coherent scattering increased to a high level when the canopy was fading at the stage of 27 August 2013.

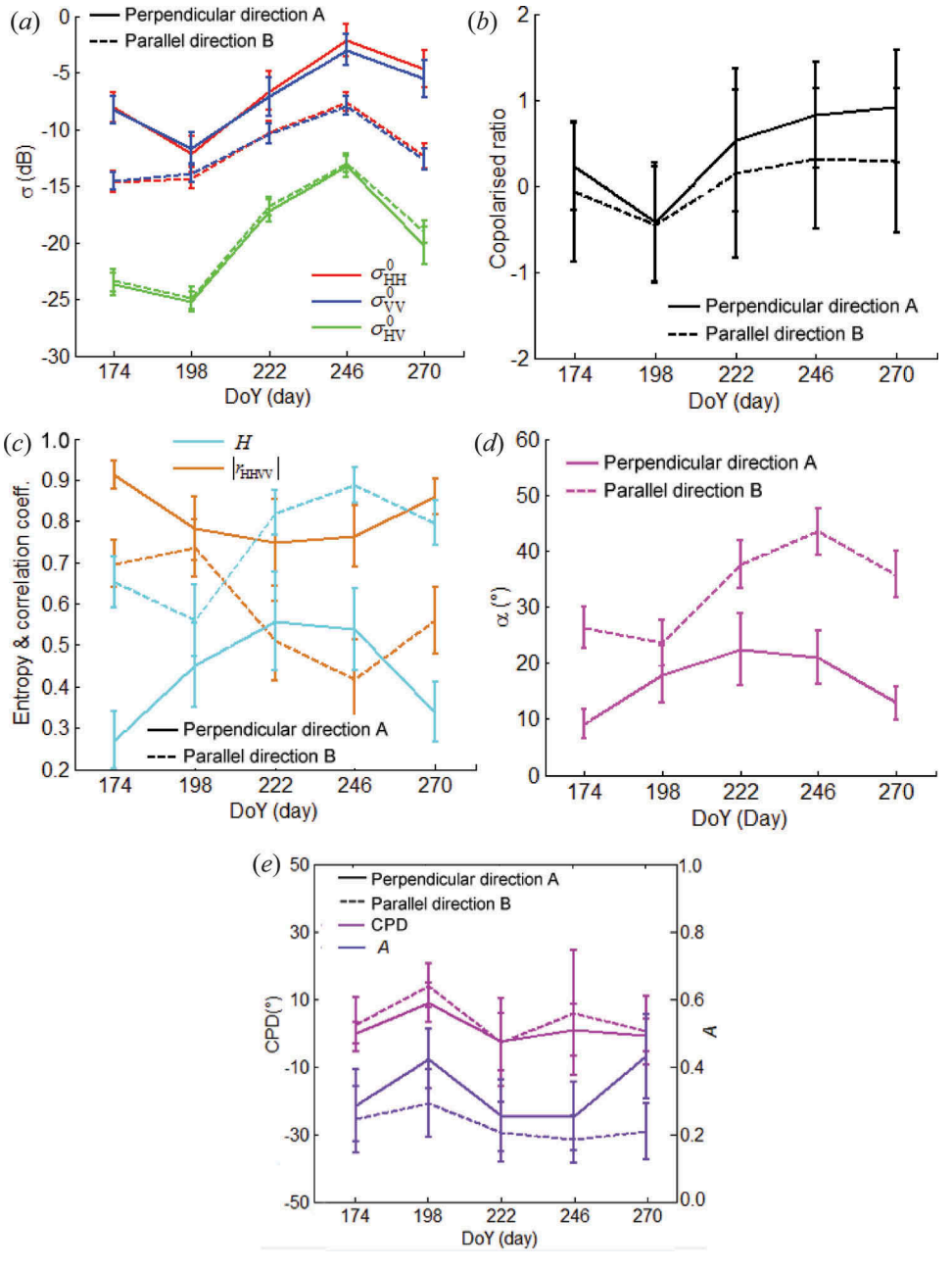

Figure 4. Evolution profiles of (a) the backscattering coefficients, (b) the copolarized ratio, (c) the entropy and copolarized correlation coefficient, (d) the alpha angle, and (e) the copolarized phase difference (CPD) and anisotropy of the periodic potato fields in different alignment directions.

Figure 4(b–e) show the evolution profiles of the composite polarimetric parameters for the potato fields. They provide insight into the understanding of the scattering mechanisms of periodic potato fields in different directions and seasons. The alpha angles of field B in parallel direction are greater than 30° at the vegetation

development stages of the potato plants. The copolarized correlation coefficients, approximating to 0.3 for pure volume scattering (Lopez–Sanchez, Cloude, and Ballester–Berman 2012), also show low values at the stages of 10 July 2013 (DoY 222) and 3 August 2013 (DoY 246). Their behaviours indicate that the scattering mechanism is dominated by the scattering from the canopy, namely volume scattering. The periodic field A in perpendicular direction has higher copolarized correlation coefficients, lower entropy and lower alpha angle values than field B in parallel direction. The alpha angle of field A is less than 30° over all the stages, indicating that the scattering mechanism is odd scattering. Consistently with the mechanism, the $|r_{HHVV}|$ of field A is larger than 0.7 and H is located in the low entropy or medium entropy zones. It is worth mentioning that the potato fields in perpendicular direction have smaller scattering randomness, and the backscattering is mainly affected by the periodic land surface.

The CPD is approaching zero for flat and volumetric scattering targets. Low values and similar pattern of CPD are observed from periodic potato fields in different directions, as shown in Figure 4(e). This is consistent with previous analysis of their scattering mechanisms. Although the enhanced coherent scattering dominates the backscattering of periodic fields in perpendicular direction, the slight higher anisotropy of field A than that of field B shown in Figure 4(e) illustrates the non-ignorable role of the contribution from canopy.

3.1.2. *The scattering characteristics of the ridging pattern induced by rows of wheat*

We selected multiple fields to analyse the coherent scattering induced by the row direction of wheat, using the data acquired at the jointing stage (14 April 2013) of wheat in Dingxing. The responses of the polarimetric signatures to the orientation angle are shown in Figure 5(a–c). Figure 5(a) shows that σ_{HH} and σ_{VV}, but not σ_{HV}, increase rapidly at a large orientation angle. Not only the intensity features, but also the polarimetric parameters such as H, $|r_{HHVV}|$ and α, show significant changes at large orientation angles, as shown in Figure 5(b,c). The cubic-polynomial is used to express their relationship, and determination coefficient (R^2) is used to measure the goodness of fit (Rogerson 2001). High determination coefficients are achieved, especially for H, $|r_{HHVV}|$ and α, as shown in Figure 5(a–c). The reduced H,increased,$|r_{HHVV}|$ and the α less than 45°, illustrate that the direction-related responses induced by vertical wheat plants are as similar as the backscatter from the periodic potato fields.

We used the dataset acquired at different phenological stages over Dingxing to investigate the changes of scattering of wheat in parallel and perpendicular directions. Multiple parallel wheat fields with orientation angles from 0° to 20°, and perpendicular fields with orientation angles between 70° and 90°, were selected. The evolution profiles of the polarimetric parameters for wheat in the parallel and perpendicular directions are shown in Figure 6(a–d). During the vegetation development stages, the backscattering of perpendicular wheat is about 2 dB higher than that of the parallel wheat at σ_{HH} and σ_{VV}, but not for σ_{HV}. The increments of σ_{HH} and σ_{VV} are similar and the γ shown in Figure 6(b) is not sensitive to the aligning direction of wheat either.

Figure 6(c) shows that the composite polarimetric parameters of H, $|r_{HHVV}|$ and α are different for the parallel and perpendicular wheat throughout all the growth stages. The

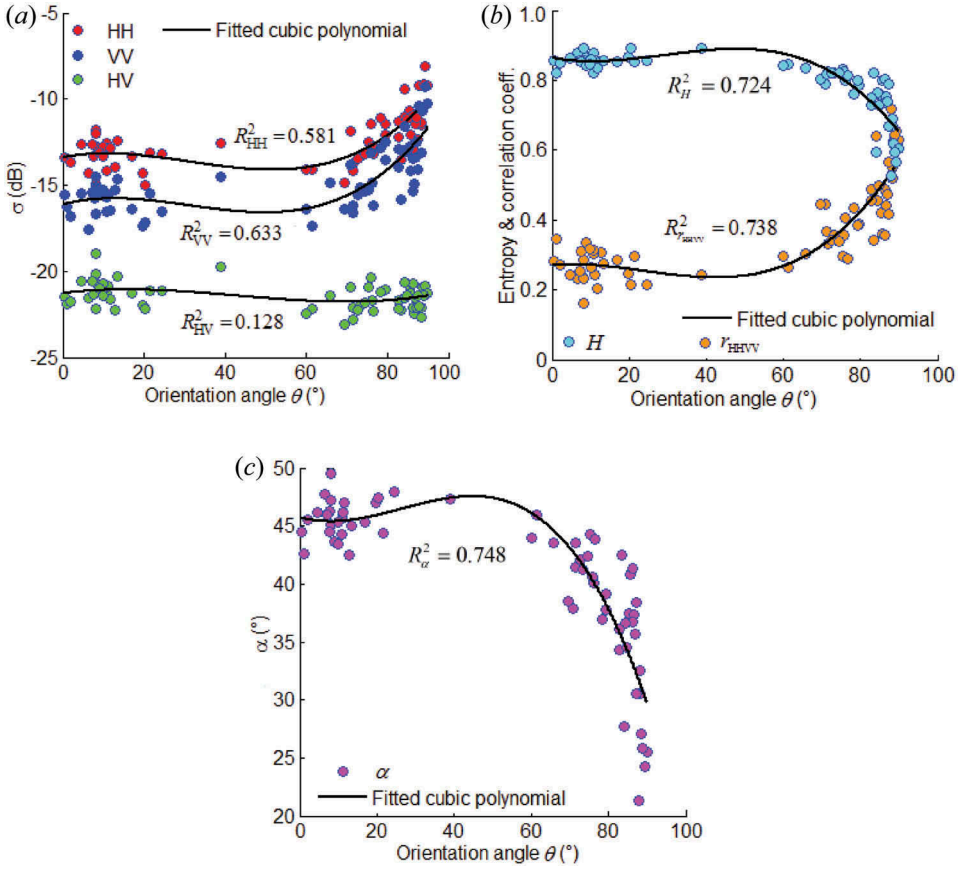

Figure 5. Changes of (a) the backscattering coefficients, (b) the entropy and copolarized correlation coefficient, and (c) the alpha angle, with orientation angle. The black curves are the fitted cubic polynomials for wheat at the stage of 14 April 2013 in Dingxing.

alpha angles of wheat in parallel direction are approaching 45°, indicating that volume scattering is the dominated scattering mechanism. The low $|r_{HHVV}|$ and the high H of parallel wheat also show the randomness of scattering. The alpha angles of wheat in perpendicular direction are lower than 45°. The slightly higher $|r_{HHVV}|$ and lower H of wheat in perpendicular direction than that of wheat in parallel direction show the effect of planting direction on reducing the scattering randomness. The anisotropy of wheat shows similar performance with that of periodic potato fields over the growth stages. A slight higher anisotropy is observed for wheat in perpendicular direction than wheat in parallel direction, because the coherent scattering induced by planting direction and volume scattering from the canopy are two main components for the backscattering of wheat in perpendicular direction. The CPD is also approaching zero for wheat in the two directions, as similar as that of periodic potato fields. It is understandable that the coherent scattering from wheat is weak at the initial tillering stage, when the row structure of wheat is not obvious. At the mature stages, the coherent backscattering is weakened by the complex structure of the wheat canopy. At a steep incidence angle, the differences in these polarimetric parameters between perpendicular and parallel

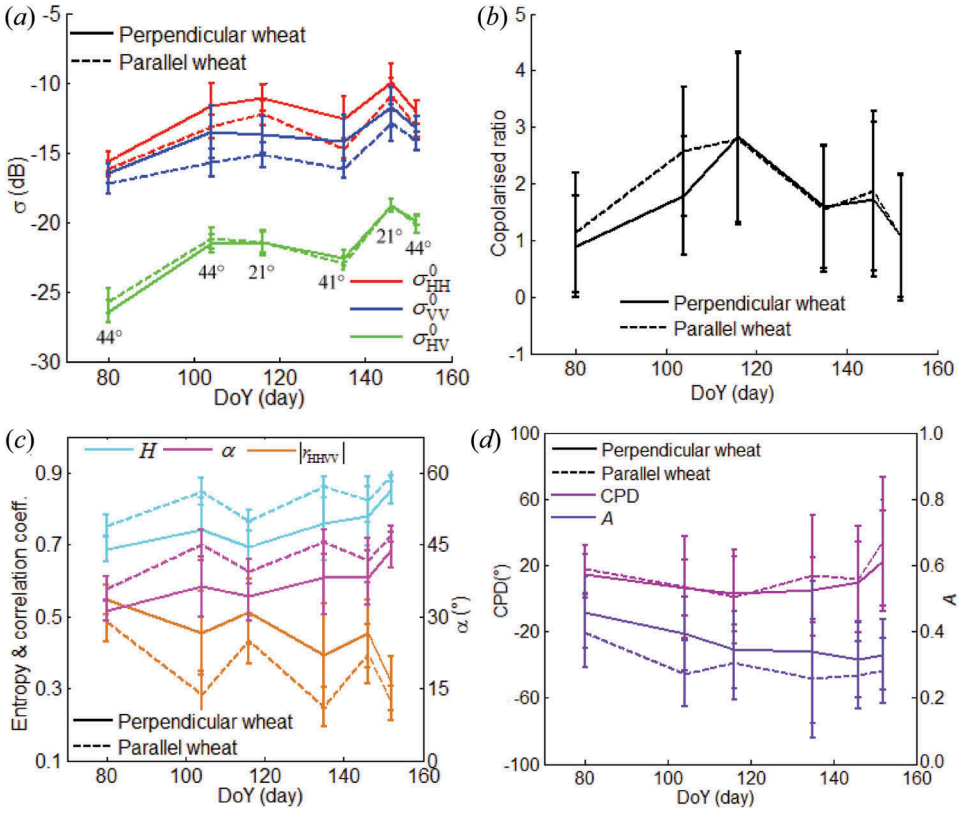

Figure 6. Evolution profiles of (a) the backscattering coefficients, (b) the copolarized ratio, (c) the entropy, copolarized correlation coefficient and alpha angle, and (d) the CPD and anisotropy of wheat in parallel and perpendicular directions in Dingxing. The incidence angles are labelled under the profile of σ_{HV}.

wheat are slightly less than those at a large incidence angle, which may be due to the reduced interaction between signal and canopy.

3.2. *The importance assessment of the polarimetric signatures for ridging pattern characterization*

Figures 7(a) and 8(b) show the classification results of the ridging directions of the potato fields and wheat using multi-temporal PolSAR images. It can be seen that the classification results are generally in agreement with the ground truths. Tables 5 and 6 show their classification accuracies by the use of confusion matrices. The overall accuracy (OA) of the classification results is 99.8% for periodic potato fields. The significantly different scattering characteristics of periodic potato fields in two directions are favour of the high classification accuracy. The overall accuracy of the classification results of wheat in two directions is 89.5%, which is lower than the classification accuracy of potato. The distinction for them is not expected as clear as the periodic potato fields, since the backscattering of wheat in different directions are all mainly come from the

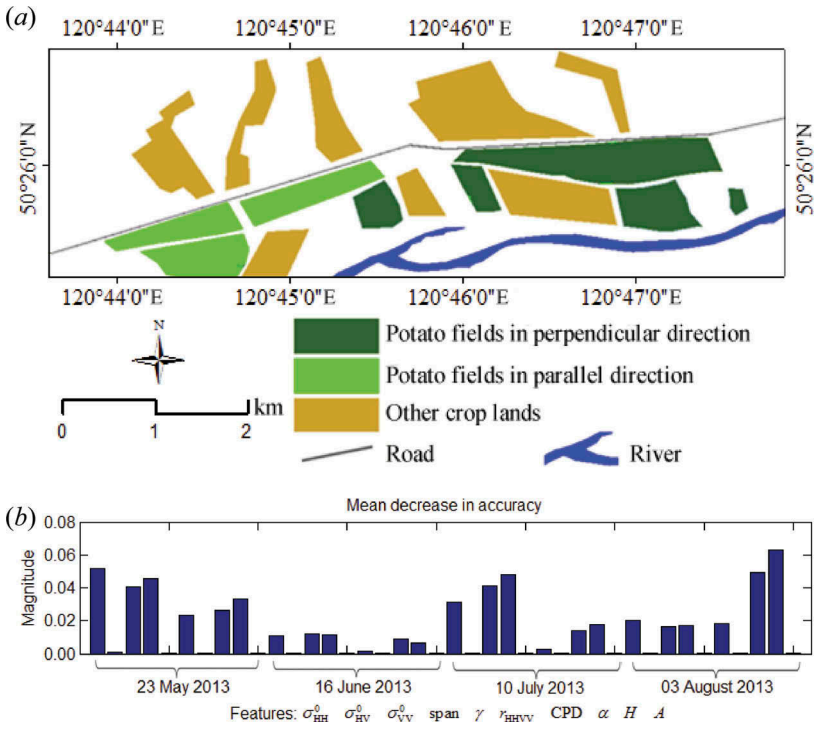

Figure 7. (a) Classification results of the periodic fields in different directions and (b) the importance scores from Random Forest (RF).

canopy. The increased randomness of the wheat canopy in the latter crop development stages reduces the direction-related scattering.

Figures 7(b) and 8(c) show the importance scores of the polarimetric parameters for the potato fields and row wheat. The σ^0_{HH}, σ^0_{VV}, span, $|r_{HHVV}|$,H and α of the periodic potato fields have relatively high scores in all four temporal stages. The polarimetric parameters for the periodic fields at the stage of 16 June 2013 have relatively low scores, because of the non-significant periodic structure. The scores of the polarimetric signatures of wheat show low fluctuation. Figure 8(c) shows that the polarimetric parameters of wheat in the jointing (14 April 2013) and flowering (15 May 2013) stages have higher scores than those in the tillering and milk ripening stages, which is consistent with the previous analysis. The parameters with relatively low importance scores are CPD,γ and A. This is because the odd scattering and volume scattering are the dominant scattering mechanisms for the ridging patterns, and the statistical means of CPD for the two types of scattering mechanisms all approach zero. The γ has relatively low importance scores, because coherent scattering makes similar contributions to σ^0_{HH} and σ^0_{VV}.

4. Conclusions

This article has documented the backscattering of ridging patterns in agriculture by taking periodic potato fields and row wheat as two examples. The behaviours of a set of polarimetric parameters show that the alignment direction of the ridging patterns is the

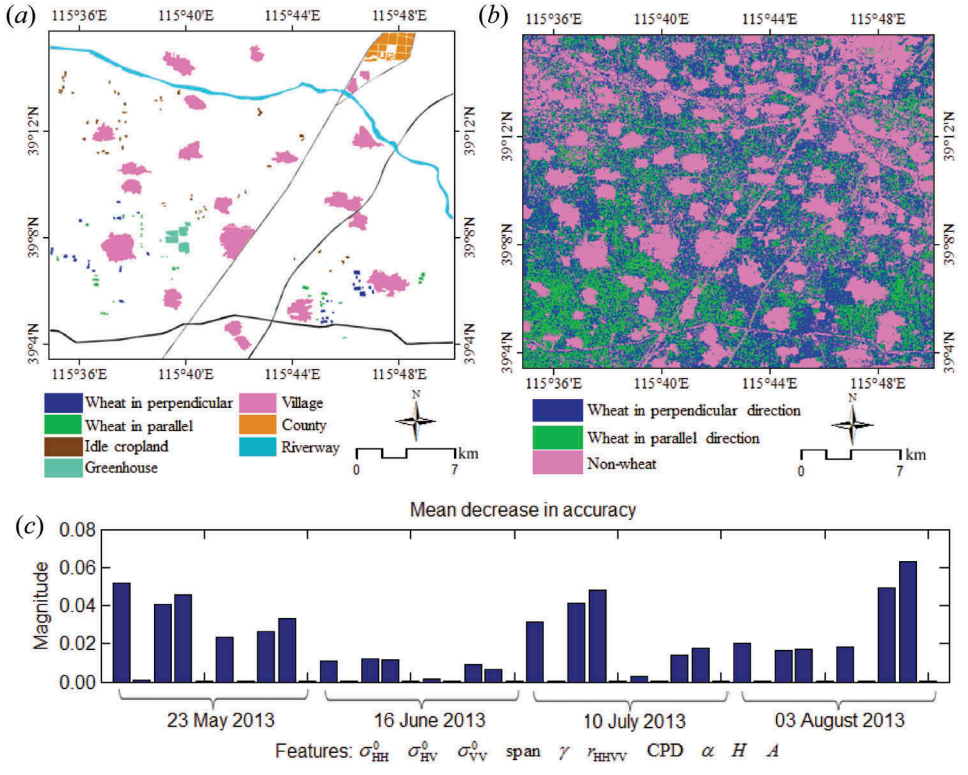

Figure 8. (a) Ground truth of the land cover in Dingxing County. (b) Classification results of wheat in different directions. (c) Importance scores derived from random forest for the classification of wheat in different directions.

Table 5. Accuracies for the classification results of potato fields in different directions.

	Potato in perpendicular direction	Potato in parallel direction	User's accuracy (%)
Potato in perpendicular direction	19,014	39	99.7
Potato in parallel direction	15	12,181	99.8
Producer's accuracy (%)	99.9	99.6	OA (99.8)

Table 6. Accuracies for the classification results of wheat in different directions.

	Wheat in perpendicular direction	Wheat in parallel direction	User's accuracy (%)
Wheat in perpendicular direction	7480	298	96.2
Wheat in parallel direction	1625	8827	84.5
Producer's accuracy (%)	82.2	96.7	OA (89.5)

key factor for coherent scattering. When the alignment direction is perpendicular to the LOS, significant coherent scattering is observed for the ridging patterns. The occurring coherent scattering has enhanced copolarized backscattering, high copolarized correlation coefficient, low entropy and low polarimetric alpha angle. This shows that the dominant

scattering mechanism of coherent scattering is odd scattering. Furthermore, the evolution profiles of the polarimetric signatures indicate that the coherent scattering makes a large contribution to the backscattering over the vegetation development stages of the crops.

The enhanced backscattering coefficients induced by the ridging patterns may hinder the accurate estimation of the physical parameters (Wegmüller et al. 2011; He et al. 2016). In addition, the coherent scattering results in the dominant scattering mechanism of the crop canopy deviating from volume scattering, which may impede the phenological monitoring of crops. However, the characterization of the ridging patterns furthers the understanding of the interaction between the signal and the ridging patterns. The conclusions made in this study will help us to develop more sophisticated techniques to weaken the effect of ridging patterns on specific applications, and to improve the capability of SAR for agriculture monitoring.

Acknowledgements

The authors would like to thank the anonymous referees for their constructive comments. This work was supported in part by the project funded by the China Post-Doctoral Science Foundation, under Grant 2016M592391, the National Natural Science Foundation of China (NSFC), under Grant 41601355, 61371199 and 41501382, the Natural Science Foundation of Hubei Province, under Grant 2016CFB246, and the National Key Research and Development Program of China, under Grant 2016YFB0502603. The authors wish to thank Prof. Quan Chen from RADI and Prof. Erxue Chen from FADI and their colleagues for the help in collecting data in the field. The Radarsat-2 images were provided by MacDonald, Dettwiler and Associates Ltd. (MDA) and the Canadian Space Agency (CSA) in the framework of project 13/783-48A/05.

Disclosure statement

No potential conflict of interest was reported by the authors.

Funding

This work was supported in part by the project funded by the China Post-Doctoral Science Foundation, under Grant [2016M592391], the National Natural Science Foundation of China (NSFC), under Grant [41601355, 61371199 and 41501382], the Natural Science Foundation of Hubei Province, under Grant [2016CFB246], and the National Key Research and Development Program of China, under Grant [2016YFB0502603].

References

Auquiere, E., P. Defourny, V. Baltazart, and A. Guissard. 1997. "ERS SAR Time Series Analysis for Maize Monitoring Using Experimental and Modeling Approaches." Proceedings of the ESA ERS Conference, Florence, Italy, March 5, 147–152.

Barrett, B., I. Nitze, S. Green, and F. Cawkwell. 2014. "Assessment of Multi-Temporal, Multi-Sensor Radar and Ancillary Spatial Data for Grasslands Monitoring in Ireland Using Machine Learning Approaches." *Remote Sensing of Environment* 152: 109–124. doi:10.1016/j.rse.2014.05.018.

Breiman, L. 2001. "Random Forests." *Machine Learning* 45: 5–32. doi:10.1023/A:1010933404324.

Brunfeldt, D. R., and F. T. Ulaby. 1986. "Microwave Emission from Row Crops." *IEEE Transactions on Geoscience and Remote Sensing* GE–24: 353–359. doi:10.1109/TGRS.1986.289592.

Cloude, S. R. 2009. *Polarisation: Applications in Remote Sensing*. London, UK: Oxford University Press.

Cloude, S. R., and E. Pottier. 1997. "An Entropy Based Classification Scheme for Land Applications of Polarimetric SAR." *IEEE Transactions on Geoscience and Remote Sensing* 35: 68–78. doi:10.1109/36.551935.

Corcione, V., F. Nunziata, L. Mascolo, and M. Migliaccio. 2016. "A Study of the Use of Cosmo-Skymed SAR Pingpong Polarimetric Mode for Rice Growth Monitoring." *International Journal of Remote Sensing* 37: 633–647. doi:10.1080/01431161.2015.1131902.

Ferrazzoli, P., S. Paloscia, P. Pampaloni, G. Schiavon, S. Sigismondi, and D. Solimini. 1997. "The Potential of Multifrequency Polarimetric SAR in Assessing Agricultural and Arboreous Biomass." *IEEE Transactions on Geoscience and Remote Sensing* 35: 5–17. doi:10.1109/36.551929.

Ferro–Famil, L., A. Reigber, E. Pottier, and W. M. Boerner. 2003. "Scene Characterization Using Subaperture Polarimetric SAR Data." *IEEE Transactions on Geoscience and Remote Sensing* 41: 2264–2276. doi:10.1109/TGRS.2003.817188.

Hajnsek, I., T. Jagdhuber, H. Schon, and K. P. Papathanassiou. 2009. "Potential of Estimating Soil Moisture under Vegetation Cover by Means of Polsar." *IEEE Transactions on Geoscience and Remote Sensing* 47: 442–454. doi:10.1109/TGRS.2008.2009642.

He, L., R. Panciera, M. A. Tanase, J. P. Walker, and Q. Qin. 2016. "Soil Moisture Retrieval in Agricultural Fields Using Adaptive Model–Based Polarimetric Decomposition of SAR Data." *IEEE Transactions on Geoscience and Remote Sensing* 54: 4445–4460. doi:10.1109/TGRS.2016.2542214.

Hosseini, M., H. Mcnairn, A. Merzouki, and A. Pacheco. 2015. "Estimation of Leaf Area Index (LAI) in Corn and Soybeans Using Multi-Polarization C- and L-Band Radar Data." *Remote Sensing of Environment* 170: 77–89. doi:10.1016/j.rse.2015.09.002.

Jagdhuber, T., I. Hajnsek, A. Bronstert, and K. P. Papathanassiou. 2013. "Soil Moisture Estimation under Low Vegetation Cover Using a Multi-Angular Polarimetric Decomposition." *IEEE Transactions on Geoscience and Remote Sensing* 51: 2201–2215. doi:10.1109/TGRS.2012.2209433.

Lee, J.-S., M. R. Grunes, and G. De Grandi. 1999. "Polarimetric SAR Speckle Filtering and Its Implication for Classification." *IEEE Transactions on Geoscience and Remote Sensing* 37: 2363–2373. doi:10.1109/36.789635.

Lee, J. S., and E. Pottier. 2009. *Polarimetric Radar Imaging: From Basics to Applications*. Boca Raton, FL: Taylor & Francis.

Loosvelt, L., J. Peters, H. Skriver, B. De Baets, and N. E. C. Verhoest. 2012. "Impact of Reducing Polarimetric SAR Input on the Uncertainty of Crop Classifications Based on the Random Forests Algorithm." *IEEE Transactions on Geoscience and Remote Sensing* 50: 4185–4200. doi:10.1109/TGRS.2012.2189012.

Lopez–Sanchez, J. M., S. R. Cloude, and J. D. Ballester–Berman. 2012. "Rice Phenology Monitoring by Means of SAR Polarimetry at X–Band." *IEEE Transactions on Geoscience and Remote Sensing* 50: 2695–2709. doi:10.1109/TGRS.2011.2176740.

Manninen, T., P. Stenberg, M. Rautiainen, and P. Voipio. 2013. "Leaf Area Index Estimation of Boreal and Subarctic Forests Using VV/HH ENVISAT/ASAR Data of Various Swaths." *IEEE Transactions on Geoscience and Remote Sensing* 51: 3899–3909. doi:10.1109/TGRS.2012.2227327.

Mascolo, L., J. M. Lopez-Sanchez, F. Vicente-Guijalba, G. Mazzarella, F. Nunziata, and M. Migliaccio. 2015. "Retrieval of Phenological Stages of Onion Fields during the First Year of Growth by Means of C-Band Polarimetric SAR Measurements." *International Journal of Remote Sensing* 36: 3077–3096. doi:10.1080/01431161.2015.1055608.

Mascolo, L., J. M. Lopez-Sanchez, F. Vicente-Guijalba, F. Nunziata, M. Migliaccio, and G. Mazzarella. 2016. "A Complete Procedure for Crop Phenology Estimation with Polsar Data Based on the Complex Wishart Classifier." *IEEE Transactions on Geoscience and Remote Sensing* 54: 6505–6515. doi:10.1109/TGRS.2016.2585744.

Mattia, F. 2011. "Coherent and Incoherent Scattering from Tilled Soil Surfaces." *Waves in Random and Complex Media* 21: 278–300. doi:10.1080/17455030.2011.552533.

Mcnairn, H., C. Duguay, B. Brisco, and T. J. Pultz. 2002. "The Effect of Soil and Crop Residue Characteristics on Polarimetric Radar Response." *Remote Sensing of Environment* 80: 308–320. doi:10.1016/S0034-4257(01)00312-1.

Moran, M. S., L. Alonso, J. F. Moreno, M. Pilar Cendrero Mateo, D. Fernando De La Cruz, and A. Montoro. 2012. "A Radarsat-2 Quad-Polarized Time Series for Monitoring Crop and Soil Conditions in Barrax, Spain." *IEEE Transactions on Geoscience and Remote Sensing* 50: 1057–1070. doi:10.1109/TGRS.2011.2166080.

Moreira, A., P. Prats-Iraola, M. Younis, G. Krieger, I. Hajnsek, and K. P. Papathanassiou. 2013. "A Tutorial on Synthetic Aperture Radar." *IEEE Geoscience and Remote Sensing Magazine* 1: 6–43. doi:10.1109/MGRS.2013.2248301.

Morena, L., K. James, and J. Beck. 2004. "An Introduction to the Radarsat–2 Mission." *Canadian Journal of Remote Sensing* 30: 221–234. doi:10.5589/m04-004.

Ouchi, K., S. Niiuchi, and K. Mohri. 1999. "On the Simulation and Observation of the Bragg Scattering in the JERS–1 SAR Images of Machine–Planted Rice Fields in the Kojima, Okayama, Japan." IEEE 1999 International Geoscience and Remote Sensing Symposium, Hamburg, Germany, June 28, 919–921.

Ponnurangam, G., T. Jagdhuber, I. Hajnsek, and Y. Rao. 2016. "Soil Moisture Estimation Using Hybrid Polarimetric SAR Data of RISAT-1." *IEEE Transactions on Geoscience and Remote Sensing* 54: 2033–2049. doi:10.1109/TGRS.2015.2494860.

Rogerson, P. 2001. *Statistical Methods for Geography*. London: Sage.

Rosenqvist, A. 1999. "Temporal and Spatial Characteristics of Irrigated Rice in JERS–1 L–Band SAR Data." *International Journal of Remote Sensing* 20: 1567–1587. doi:10.1080/014311699212614.

Shin, R. T., and J. A. Kong. 1984. "Scattering of Electromagnetic Waves from a Randomly Perturbed Quasiperiodic Surface." *Journal of Applied Physics* 56: 10–21. doi:10.1063/1.333743.

Ulaby, F. T., D. G. Long, W. J. Blackwell, C. Elachi, A. K. Fung, C. Ruf, K. Sarabandi, H. A. Zebker, and J. J. vanZyl. 2014. *Microwave Radar and Radiometric Remote Sensing*. America: University of Michigan Press.

vanZyl, J. J., and Y. J. Kim. 2011. *Synthetic Aperture Radar Polarimetry*. Hoboken, NJ: John Wiley & Sons.

Wegmüller, U., R. A. Cordey, C. Werner, and P. J. Meadows. 2006. "'Flashing Fields' in Nearly Simultaneous ENVISAT and ERS–2 C–Band SAR Images." *IEEE Transactions on Geoscience and Remote Sensing* 44: 801–805. doi:10.1109/TGRS.2005.861479.

Wegmüller, U., M. Santoro, F. Mattia, A. Balenzano, G. Satalino, P. Marzahn, G. Fischer, R. Ludwig, and N. Floury. 2011. "Progress in the Understanding of Narrow Directional Microwave Scattering of Agricultural Fields." *Remote Sensing of Environment* 115: 2423–2433. doi:10.1016/j.rse.2011.04.026.

Xie, L., H. Zhang, H. Li, and C. Wang. 2015. "A Unified Framework for Crop Classification in Southern China Using Fully Polarimetric, Dual Polarimetric, and Compact Polarimetric SAR Data." *International Journal of Remote Sensing* 36: 3798–3818. doi:10.1080/01431161.2015.1070319.

Zeyada, H. H., M. M. Ezz, A. H. Nasr, M. Shokr, and H. M. Harb. 2016. "Evaluation of the Discrimination Capability of Full Polarimetric SAR Data for Crop Classification." *International Journal of Remote Sensing* 37: 2585–2603. doi:10.1080/01431161.2016.1182663.

Zhao, L., J. Yang, P. Li, and L. Zhang. 2014a. "Characteristics Analysis and Classification of Crop Harvest Patterns by Exploiting High–Frequency Multipolarization SAR Data." *IEEE Journal of Selected Topics in Applied Earth Observations and Remote Sensing* 7: 3773–3783. doi:10.1109/JSTARS.2014.2308273.

Zhao, L., J. Yang, P. Li, and L. Zhang. 2014b. "Seasonal Inundation Monitoring and Vegetation Pattern Mapping of the Erguna Floodplain by Means of a Radarsat-2 Fully Polarimetric Time Series." *Remote Sensing of Environment* 152: 426–440. doi:10.1016/j.rse.2014.06.026.